Power-Synchronization Control of Grid-Connected Voltage-Source Converters

Lidong Zhang, *Member, IEEE*, Lennart Harnefors, *Senior Member, IEEE*, and Hans-Peter Nee, *Senior Member, IEEE*

***Abstract*—In this paper, a novel control method of grid-connected voltage-source converters (VSCs) is proposed. The method can be generally applied for all grid-connected VSCs but may be of most importance in high-voltage dc (HVDC) applications. Different from the previous control methods, the proposed method utilizes the internal synchronization mechanism in ac systems, in principle, similar to the operation of a synchronous machine. By using this type of power-synchronization control, the VSC avoids the instability caused by a standard phase-locked loop in a weak ac-system connection. Moreover, a VSC terminal can give the weak ac system strong voltage support, just like a normal synchronous machine does. The control method is verified by both analytical models and time simulations.**

***Index Terms*—Control, converters, HVDC, phase-locked loops, power systems, stability.**

I. Introduction

PULSEWIDTH-MODULATION (PWM)-based voltage-source converter (VSC) techniques have been widely used in grid-connected applications, such as adjustable-speed drives (ASDs) with PWM rectifiers, power quality improvement, wind turbines, etc. [1]. Thanks to the gradually increased rating and reduced costs, they have also been applied for high-voltage dc (HVDC) transmission in recent years [2]. Compared to the conventional thyristor-based HVDC, VSC-HVDC has a number of technical merits: reactive-power support to the ac system, possibility to connect to very weak ac systems, black-start capability, and lower cable cost, just to name a few.

Several control methods of grid-connected VSCs have been proposed. Among them, power-angle control and vector-current control are the two that have been mostly investigated [3]. The principle of power-angle control is fairly simple and easily implemented. The active power is controlled by the phase-angle shift between the VSC and the ac system, while the reactive power is controlled by varying the VSC voltage magnitude [4]. Power-angle control has been studied for HVDC, static-synchronous-compensator (STATCOM), and wind-turbine applications [5], [6]. One disadvantage of power-angle control is that the control bandwidth is limited by a resonant peak at the grid frequency [6]. Another disadvantage is that the control system does not have the capability to limit the current flowing into the converter [7]. The latter is a serious problem, as VSCs usually do not have an over-current capability. In high-power applications, it is highly important for the control to limit the valve current to prevent the converter from being blocked (tripped) at disturbances.

Vector-current control [6] is a current-control-based technology. Thus, it can naturally limit the current flowing into the converter during disturbances. The basic principle of vector-current control is to control the instantaneous active power and reactive power independently through a fast inner current control loop. By using a dq decomposition technique with the grid voltage as phase reference, the inner current control loop decouples the current into d and q components, where outer loops can use the d component to control active power or direct voltage, and the q component to control reactive power or alternating voltage. Due to its successful application in ASDs, doubly-fed induction-generator (DFIG) wind turbines, etc., vector-current control has become the dominant control method for grid-connected VSCs in almost all applications today [8].

Interestingly, as one of the original purposes to use VSCs for HVDC applications was its possibility to connect to very weak ac systems, where the conventional thyristor-based HVDC is not applicable, some difficulties have been experienced by VSC-HVDC based on vector-current control in weak ac-system connections [9], [10]. One of the problems is the low-frequency resonance that is typically present. This can interfere with the fast inner current control loop, thereby limiting the VSC control performance [7], [11]. The other one has to do with the phase-locked loop (PLL). In almost all VSCs connected to ac systems, a PLL is used to obtain an accurate synchronization to the ac system [12]. This has since long been believed to be a pre-condition for any grid-connected VSC. However, several investigations have shown that the PLL dynamics might have a negative impact on the performance of VSC-HVDC in weak ac-system connections [9], [11], [13].

This paper proposes a new synchronization method, the so-called power synchronization, as an alternative to a normal PLL. In some way, power-synchronization control is similar to power-angle control, e.g., using phase angle and voltage magnitude to directly control active power and reactive power. However, a major difference is that no PLL is needed in power-synchronization control. Besides, typical problems with power-angle control, such as the resonant peak at grid frequency and converter over-current limitation, are properly treated in the proposed control. The latter, in fact, is similar to vector-current control.

Manuscript received January 28, 2009; revised August 15, 2009. First published November 03, 2009; current version published April 21, 2010. This work was supported by ELFORSK under the Electra program. Paper no. TPWRS-00063-2009.

L. Zhang and L. Harnefors are with ABB Power Systems, SE-771 80 Ludvika, Sweden (e-mail: lidong.zhang@se.abb.com; lennart.harnefors@se.abb.com).

H.-P. Nee is with the School of Electrical Engineering, Royal Institute of Technology, SE-100 44 Stockholm, Sweden (e-mail: hansi@ee.kth.se).

Digital Object Identifier 10.1109/TPWRS.2009.2032231

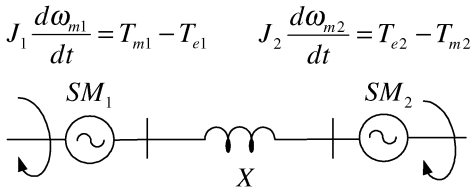

Fig. 1. Synchronization mechanism between SMs in an ac system.

The paper is organized as follows. In Section II, the power-synchronization concept is illustrated by a small power system, and a power-synchronization control law for VSCs is proposed. In Section III, the transfer functions of active power versus load angle, and reactive power versus voltage magnitude are derived. In Section IV, the overall controller design based on power synchronization is described. In Section V, the proposed control design and analytical model are verified by a VSC-HVDC link model in PSCAD.

II. Concept of Power Synchronization

A. Power-Synchronization Mechanism Between Synchronous Machines

In this subsection, the power-synchronization mechanism between synchronous machines (SMs) in ac systems is described. The mechanism is illustrated by a simple system consisting of two interconnected SMs as shown in Fig. 1. SM_1 operates as a generator and SM_2 operates as a motor. The reactance X is the sum of the reactances of the SMs and that of the line interconnecting the two SMs. All resistances and other damping effects are disregarded.

Initially, it is assumed that the two SMs operate at steady state. Two phasors E_1 and E_2 represent the line-to-line equivalents of the inner emfs of the two SMs, respectively. These emfs are assumed to be constant at all times (even during transients). The electric power transmitted from SM_1 to SM_2 is given by

$$P = \frac{E_1 E_2 \sin\theta}{X} \tag{1}$$

where θ is the electrical angle separating the two emfs E_1 and E_2. The mechanical torque T_{m1} of SM_1 is now increased by a certain amount for a short duration and then brought back to its initial value. As a consequence of the temporary increase of T_{m1}, the mechanical angle of the rotor of SM_1 advances, as predicted by the generator-mode swing equation

$$J_1 \frac{d\omega_{m1}}{dt} = T_{m1} - T_{e1} \tag{2}$$

where J_1 is the total inertia of the shaft-system of SM_1, ω_{m1} is the rotor speed, and T_{e1} is the electromagnetic torque of SM_1. Since the emf of a synchronous machine is tightly connected to the rotor position, the advance of the mechanical angle of the rotor of SM_1 inevitably causes an advance of the phase of the emf of SM_1. Due to the phase advancement of E_1, the phase difference between the emfs of the two SMs is increased. According to (2), *this translates into an increase of the electric power transmitted from SM_1 to SM_2*. This increase in power is equivalent to an increase in the electromagnetic torque T_{e2} of SM_2. Assuming that SM_2 has a constant load torque T_{m2}, the rotor of SM_2 starts to accelerate as dictated by

$$J_2 \frac{d\omega_{m2}}{dt} = T_{e2} - T_{m2} \tag{3}$$

where J_2 is the total inertia of the shaft-system of SM_2, and ω_{m2} is the mechanical angular velocity of SM_2. As the rotor of SM_2 starts to accelerate, the same thing occurs with the phase of E_2. The acceleration of the phasor E_2 results in a reduction of the phase difference between the emfs of the two SMs. After a transient, which in reality involves a certain amount of damping, the phase difference between the emfs of the two SMs is brought back to its initial value (as the transmitted electric power), and the system is again at steady state.

The example shows that if the emf of one SM changes its angular position, the other SM will follow in order to maintain synchronism. This synchronization mechanism is known to all power system specialists. The important observation to make here, however, is that *the synchronization process is achieved by means of a transient power transfer*. The same kind of synchronization also appears in large systems of interconnected synchronous machines. Due to the fact that synchronous machines can stay in synchronism in cases where vector controlled VSCs are prone to fail, it makes sense to suggest a control method based on a synchronization process where the electric power is the communicating medium. Since the mechanical angular velocity ω_m is the derivative of the angular position, (2) represents a double integration when going from torque (or electric power) to angular position. This double integration, inherently, yields a poor phase margin even with considerable damping. In the next subsection, therefore, a controller based on power synchronization employing only a single integration is suggested.

B. Power-Synchronization Control of VSCs

From the discussion in the preceding subsection, it is known that the SMs in an ac system maintain synchronism by means of *power synchronization*, i.e., a transient power transfer. This power transfer involves a current which is determined by the interconnecting network. Generally, this current is unknown. If power-synchronization should be used to control a VSC, therefore, it cannot be combined with a vector-current controller, which requires a *known* current reference. As will be shown below, the active power output from the VSC is instead controlled directly by the power-synchronization loop and the reactive power (or alternating voltage) is controlled by adjusting the magnitude of the voltage. Consequently, an inner current loop is not necessary. The only exception is during severe ac system faults. In such cases, the control system needs to switch to the current-control mode in order to prevent over-current of the converter valves. Meanwhile, a backup PLL is applied to provide synchronization. This issue is addressed in Section IV-F. The

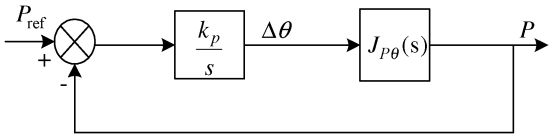

Fig. 2. Active-power control block diagram of a VSC using power-synchronization control.

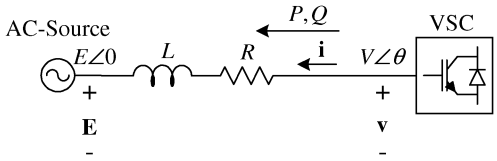

Fig. 3. Simplified VSC-ac system connection for dynamic analysis.

power-synchronization control law for VSCs is now proposed as

$$\frac{d\Delta\theta}{dt} = k_p(P_{\text{ref}} - P) \tag{4}$$

where P_{ref} is the reference for the active power, P is the measured active power output from the VSC, k_p is the controller gain, and $\Delta\theta$ is the output of the controller. As already mentioned above, $\Delta\theta$ directly provides the synchronization for the VSC. An additional PLL is obviously not necessary during normal operation. The dynamic process of a VSC using power-synchronization control is very similar to that of interconnected SMs. The transmitted power is increased or decreased by shifting the output voltage phasor of the VSC forwards or backwards. The design of the power-synchronization loop is described in detail in Section IV.

The proposed control law is not an exact copy of the swing equation of an SM. In the SM case, the change of the electrical angle from the power reference involves the governor and turbine-rotor dynamics, while for the VSC, it is easily achieved by a simple integration process. In Fig. 2, the block diagram of the power-synchronization control loop is shown. The transfer function $J_{\text{P}\theta}(s)$ is the ac system transfer function from $\Delta\theta$ to ΔP. This transfer function is derived in Section III-A.

III. Transfer Functions of Active Power versus Load Angle and Reactive Power versus Voltage Magnitude

Consider an ac system where two nodes, having the line-to-line voltages E and V, respectively, are interconnected by a line with the reactance X. In steady state, the active power P and reactive power Q from the node with the voltage V are given by the well-known relations

$$P = \frac{EV\sin\theta}{X} \tag{5}$$

$$Q = \frac{V^2 - EV\cos\theta}{X} \tag{6}$$

where θ is the load angle between the two nodes. Active power versus load angle and reactive power versus voltage magnitude are two of the most important dynamic relations in power systems. However, due to historical reasons and to the comparably slow dynamic processes of traditional power systems (with a negligible amount of power electronic devices), these two dynamic relations are often analyzed using so-called quasi-static methods [14], which basically take the partial differential on (5) with θ, and (6) with V. Thus

$$\frac{\partial P}{\partial\theta} = \frac{EV\cos\theta}{X} \tag{7}$$

$$\frac{\partial Q}{\partial V} = \frac{2V - E\cos\theta}{X}. \tag{8}$$

Quasi-static analysis is only useful for relatively slow dynamic processes, and gives qualitative results, since the network electromagnetic transient is not considered in the equations. To analyze fast power components, such as power electronic devices, the electromagnetic transient is vital for the control performance. Thus, more rigorous mathematical transfer functions are needed. In this section, the transfer functions of active power versus load angle, and reactive power versus voltage magnitude are derived based on Kirchhoff's voltage law and space vector theory. Fig. 3 shows a simplified VSC-ac system connection, where the ac-system impedance and VSC phase reactor are lumped together and represented by an inductor L and resistor R. The space vector of the ac-source voltage $\mathbf{E}^s$ and the VSC voltage $\mathbf{v}^s$ are given by

$$\begin{aligned}\mathbf{E}^s &= \frac{2}{3}\left(e_a + e^{j\frac{2\pi}{3}}e_b + e^{j\frac{4\pi}{3}}e_c\right)\\ \mathbf{v}^s &= \frac{2}{3}\left(v_a + e^{j\frac{2\pi}{3}}v_b + e^{j\frac{4\pi}{3}}v_c\right)\end{aligned} \tag{9}$$

where

$$\begin{aligned}e_a &= E\cos(\omega_1 t)\\ e_b &= E\cos\left(\omega_1 t - \frac{2\pi}{3}\right)\\ e_c &= E\cos\left(\omega_1 t - \frac{4\pi}{3}\right)\\ v_a &= V\cos(\omega_1 t + \theta)\\ v_b &= V\cos\left(\omega_1 t - \frac{2\pi}{3} + \theta\right)\\ v_c &= V\cos\left(\omega_1 t - \frac{4\pi}{3} + \theta\right).\end{aligned} \tag{10}$$

ω_1 is defined as the angular synchronous frequency of the ac source. The superscript s denotes the stationary reference frame, i.e., a reference frame with the real axis aligned with e_a. Consequently, the ac source has zero initial phase angle, while the VSC is assumed to lead the ac source by the load angle θ. P and Q represent the active and reactive power outputs from the VSC and $\mathbf{i}$ is the alternating current vector from the VSC.

A. Transfer Function of Active Power versus Load Angle

To start, the voltage control law for the VSC is given by

$$\mathbf{v}_{\text{ref}}^{c} = V \tag{11}$$

where superscript c denotes the converter dq frame, i.e., a rotating reference frame with the d axis aligned with the vector $\mathbf{v}^s$. Equation (11) is the simplest control mode. Physically, it can be interpreted as that the VSC simply produces a sinusoidal waveform with the voltage magnitude V. The active power is controlled by moving the load angle forwards or backwards by the power-synchronization law (4).

If the three-phase system is symmetrical, the dynamic equation in Fig. 3 can be described by Kirchhoff's voltage law as

$$L\frac{d\mathbf{i}^s}{dt} = \mathbf{v}^s - \mathbf{E}^s - R\mathbf{i}^s. \tag{12}$$

Equation (12) can be transformed into a rotating reference frame with the d axis aligned with $\mathbf{E}^s$. This is achieved by using the relations

$$\mathbf{E}^s = \mathbf{E}e^{j\omega_1 t}, \qquad \mathbf{i}^s = \mathbf{i}e^{j\omega_1 t}, \qquad \mathbf{v}^s = \mathbf{v}e^{j\omega_1 t}. \tag{13}$$

Substituting (13) into (12) yields the dynamic equation in the ac-source dq frame

$$L\frac{d\mathbf{i}}{dt} = \mathbf{v} - \mathbf{E} - R\mathbf{i} - j\omega_1 L\mathbf{i}. \tag{14}$$

The converter dq frame leads the ac-source dq frame by the load angle θ. If the switching-time delay is neglected and it is assumed that $|\mathbf{v}_{\text{ref}}^{c}|$ does not exceed the maximum voltage modulus, then $\mathbf{v} = \mathbf{v}_{\text{ref}}^{c}e^{j\theta}$. Equation (14) can be written in component form. Thus

$$\begin{aligned} L\frac{di_d}{dt} &= V\cos\theta - E - Ri_d + \omega_1 Li_q \\ L\frac{di_q}{dt} &= V\sin\theta - Ri_q - \omega_1 Li_d. \end{aligned} \tag{15}$$

Let the voltage magnitude of the VSC be kept constant, i.e., $V = V_0$. If the operating points in (15) are denoted with subscript "0", and small-signal deviation parts are added on i_d, i_q, and θ around the operating points, it is found that

$$\theta = \theta_0 + \Delta\theta, \quad i_d = I_{d0} + \Delta i_d, \quad i_q = I_{q0} + \Delta i_q. \tag{16}$$

The cosine and sine functions are linearized as

$$\begin{aligned} \sin(\theta_0 + \Delta\theta) &\approx \sin\theta_0 + \cos\theta_0\Delta\theta \\ \cos(\theta_0 + \Delta\theta) &\approx \cos\theta_0 - \sin\theta_0\Delta\theta. \end{aligned} \tag{17}$$

Substituting (16) and (17) into (15), and keeping only the deviation parts yields the linearized form of (15)

$$\begin{aligned} L\frac{d\Delta i_d}{dt} &= -V_0\sin\theta_0\Delta\theta - R\Delta i_d + \omega_1 L\Delta i_q \\ L\frac{d\Delta i_q}{dt} &= V_0\cos\theta_0\Delta\theta - R\Delta i_q - \omega_1 L\Delta i_d \end{aligned} \tag{18}$$

where the variation in ω_1 is disregarded based on experience from numerical simulations. By applying Laplace transform to (18), the transfer functions of Δi_d versus $\Delta\theta$ and Δi_q versus $\Delta\theta$ are obtained as

$$\begin{aligned} \Delta i_d &= V_0\frac{\omega_1 L\cos\theta_0 - (sL+R)\sin\theta_0}{(sL+R)^2 + (\omega_1 L)^2}\Delta\theta \\ \Delta i_q &= V_0\frac{\omega_1 L\sin\theta_0 + (sL+R)\cos\theta_0}{(sL+R)^2 + (\omega_1 L)^2}\Delta\theta. \end{aligned} \tag{19}$$

Assuming p.u. quantities, the instantaneous active power from the VSC is given by

$$P = \text{Re}\{\mathbf{v}\mathbf{i}^*\}. \tag{20}$$

Linearizing (20) yields the expression for the active power deviation

$$\Delta P = \text{Re}\left\{\mathbf{i}_0^*\Delta\mathbf{v} + \mathbf{v}_0\Delta\mathbf{i}^*\right\} \tag{21}$$

or in component form

$$\Delta P = \begin{bmatrix} I_{d0} \\ I_{q0} \end{bmatrix}^{\text{T}} \begin{bmatrix} \Delta v_d \\ \Delta v_q \end{bmatrix} + \begin{bmatrix} V_{d0} \\ V_{q0} \end{bmatrix}^{\text{T}} \begin{bmatrix} \Delta i_d \\ \Delta i_q \end{bmatrix}. \tag{22}$$

The current $\mathbf{i}_0$ is given by

$$\mathbf{i}_0 = \frac{\mathbf{v}_0 - \mathbf{E}_0}{R + j\omega_1 L} \tag{23}$$

which has the d and q components

$$\begin{aligned} I_{d0} &= \frac{V_0\sin\theta_0}{\omega_1 L} \\ I_{q0} &= \frac{E_0 - V_0\cos\theta_0}{\omega_1 L} \end{aligned} \tag{24}$$

where the resistance R in (23) has been neglected in (24) for simplicity. In high-power electronic applications, the resistance R is usually very low, and the effect can often be neglected. At first sight, this does not seem to be consistent with the expression of Δi_d and Δi_q in (19), where R was included. However, as a high-pass current controller, which emulates a resistance R, is introduced later, it makes sense to keep R in (19).

The d and q components of the VSC voltage vector $\mathbf{v}$ at the operating point, $\mathbf{v}_0 = V_{d0} + jV_{q0}$, can be expressed as

$$V_{d0} = V_0 \cos\theta_0, \qquad V_{q0} = V_0 \sin\theta_0. \tag{25}$$

The voltage deviation parts Δv_d and Δv_q can be derived from (14). By linearization and subdivision into real and imaginary components, it is found that

$$\begin{aligned} \Delta v_d &= sL\Delta i_d - \omega_1 L\Delta i_q \\ \Delta v_q &= sL\Delta i_q + \omega_1 L\Delta i_d. \end{aligned} \tag{26}$$

The resistance R is neglected also in (26) to simplify the expression. By substituting (19), (24), (25), and (26) into (22), the linearized dynamic relation between the active power and the load angle is obtained as

$$\Delta P = \underbrace{\frac{a_0 s^2 + a_1 s + a_2}{(sL+R)^2 + (\omega_1 L)^2}}_{J_{\mathrm{P}\theta}(s)} \Delta\theta \tag{27}$$

where

$$\begin{aligned} a_0 &= \frac{L}{\omega_1}\left(E_0 V_0 \cos\theta_0 - V_0^2\right) \\ a_1 &= \frac{R}{\omega_1}\left(E_0 V_0 \cos\theta_0 - V_0^2\right) \\ a_2 &= \omega_1 L E_0 V_0 \cos\theta_0 - R E_0 V_0 \sin\theta_0. \end{aligned} \tag{28}$$

Equation (27) shows that, by power-angle control, the open-loop system has a pair of complex poles

$$s = -\frac{R}{L} \pm j\omega_1 \tag{29}$$

which are located in the left half plane. It is also interesting to notice that the quasi-static (7) is a special condition of (27) if $R = 0$ and $s = 0$ are substituted in (27).

If the resistance R is neglected in (28), $a_1 = 0$. This means that $J_{\mathrm{P}\theta}(s)$ has two symmetrical zeros

$$s = \pm\sqrt{-\frac{a_2}{a_0}} = \pm\omega_1\sqrt{\frac{E_0\cos\theta_0}{V_0 - E_0\cos\theta_0}}. \tag{30}$$

The poles of $J_{\mathrm{P}\theta}(s)$ are determined only by the resistance R and inductance L. However, the locations of the zeros of $J_{\mathrm{P}\theta}(s)$ do not depend directly on the parameters of the power systems. Instead, E_0, V_0, and θ_0 are the decisive quantities. The locations of the zeros of $J_{\mathrm{P}\theta}(s)$ can be divided by the following borders.

- The border where the zeros of $J_{\mathrm{P}\theta}(s)$ reach the origin. This is equivalent to

$$E_0 \cos\theta_0 = 0 \tag{31}$$

  i.e., $\theta_0 = \pm 90°$.
- The border where $J_{\mathrm{P}\theta}(s)$ has zeros at infinity. This is equivalent to

$$V_0 - E_0 \cos\theta_0 = 0 \tag{32}$$

  giving

$$\theta_0 = \pm \arccos\left(\frac{V_0}{E_0}\right). \tag{33}$$

- The border where $J_{\mathrm{P}\theta}(s)$ has real zeros at $\pm\omega_1$. This is equivalent to

$$\frac{E_0\cos\theta_0}{V_0 - E_0\cos\theta_0} = 1 \tag{34}$$

  giving

$$\theta_0 = \pm \arccos\left(\frac{V_0}{2E_0}\right). \tag{35}$$

  The $\pm\omega_1$ border gives an idea about how much the zeros limit the achievable bandwidth of the control system, even though it is not a "real border."

Fig. 4 shows the above-mentioned borders. For VSC-HVDC connected to weak ac systems, the operating point of the VSC is likely to be in the region where $J_{\mathrm{P}\theta}(s)$ has real zeros ($V_0/E_0 > 1$). If the resistance R is neglected, $J_{\mathrm{P}\theta}(s)$ has two symmetrical zeros, one in the left half plane (LHP) and the other in the right half plane (RHP). According to the control theory, an LHP zero can be easily compensated by the controller, but not the one in the RHP, which always represents an additional time delay [15]. From Fig. 4, it is clearly seen how the load angle θ_0 and the voltage magnitude V_0 of the VSC affect the locations of the zeros. Basically, higher load angle θ_0 and higher VSC voltage magnitude V_0 correspond to zeros closer to the origin, which means more time delays introduced by the RHP zero to the system. By crossing the origin, i.e., $\theta_0 = \pm 90°$, it is no longer possible to control the active power by the load angle, since an increased load angle $\Delta\theta$ will cause a decreased power ΔP.

As mentioned before, in VSC-HVDC applications, the resistance R is usually very low. Thus, the grid-frequency resonant poles of (29), as well as other resonances in the ac system, have to be damped out by the control system. Therefore, the voltage control law in (11) is modified as

$$\mathbf{v}_{\mathrm{ref}}^c = V_0 - H_{\mathrm{HP}}(s)\mathbf{i}^c \tag{36}$$

where $H_{\mathrm{HP}}(s)$ is a high-pass filter described by

$$H_{\mathrm{HP}}(s) = \frac{k_v s}{s + \alpha_v}. \tag{37}$$

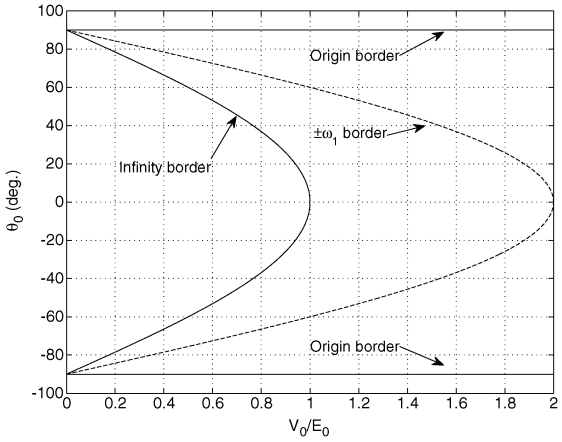

Fig. 4. Locations of zeros of $J_{P\theta}(s)$.

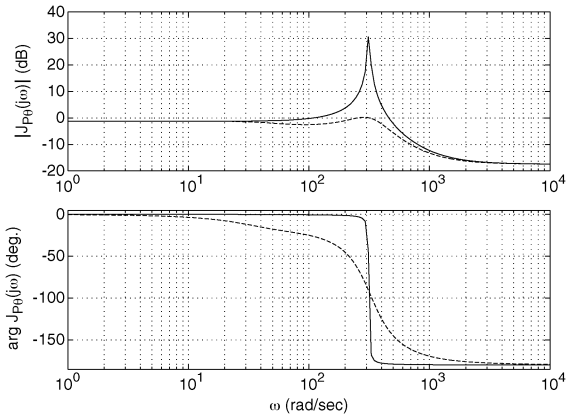

Fig. 5. Bode diagram of $J_{\mathrm{P}\theta}(s)$ and $J_{\mathrm{P}\theta-\mathrm{HP}}(s)$, $E_0 = 1.0$ p.u., $V_0 = 1.0$ p.u., $\theta_0 = 30°$, $L = 1.0$ p.u., $R = 0.01$ p.u. (solid: $J_{P\theta}(s)$, dashed: $J_{\mathrm{P}\theta-\mathrm{HP}}(s)$, $\alpha_v = 40\,\mathrm{rad/s}$, $k_v = 0.477$ p.u.).

By using the new voltage control law (36) in (14), the new active-power versus load-angle transfer function including $H_{\mathrm{HP}}(s)$ is found to be

$$\Delta P = \underbrace{\frac{a_0 s^2 + a_1 s + a_2}{\left(sL + R + H_{\mathrm{HP}}(s)\right)^2 + (\omega_1 L)^2}}_{J_{\mathrm{P}\theta-\mathrm{HP}}(s)} \Delta\theta \tag{38}$$

where

$$\begin{aligned} a_0 &= \frac{L}{\omega_1}\left(E_0 V_0 \cos\theta_0 - V_0^2\right) \\ a_1 &= \frac{\left(R + H_{\mathrm{HP}}(s)\right)}{\omega_1}\left(E_0 V_0 \cos\theta_0 - V_0^2\right) \\ a_2 &= \omega_1 L E_0 V_0 \cos\theta_0 - \left(R + H_{\mathrm{HP}}(s)\right) E_0 V_0 \sin\theta_0. \end{aligned} \tag{39}$$

The Bode diagrams of $J_{\mathrm{P}\theta}(s)$ and $J_{\mathrm{P}\theta-\mathrm{HP}}(s)$ in Fig. 5 show the damping effect of the high-pass current control part $H_{\mathrm{HP}}(s)$, which basically behaves as an "active resistor," and provides damping to the various resonances in the system, but does not consume power. The parameters of $H_{\mathrm{HP}}(s)$ are chosen based on the trade-off between the damping effect and the phase margin.

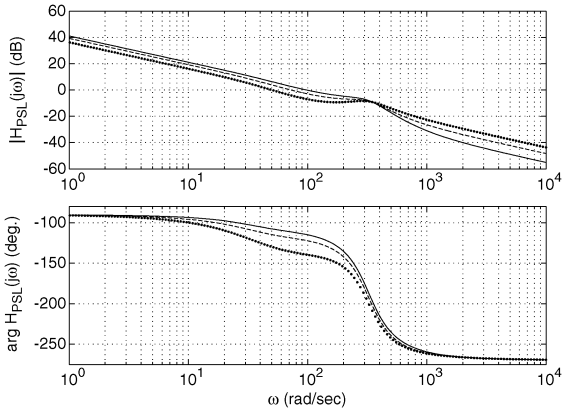

Fig. 6. Bode diagram of the open-loop transfer function $H_{\mathrm{PSL}}(s)$ of the power-synchronization loop versus different load angles, $k_p = 130\,\mathrm{rad/s}$ (solid: $\theta_0 = 30°$, dashed: $\theta_0 = 45°$, dotted: $\theta_0 = 60°$).

By analyzing the transfer function $J_{\mathrm{P}\theta-\mathrm{HP}}(s)$, the stability margin of the power-synchronization loop (PSL) can be evaluated by its open-loop transfer function

$$H_{\mathrm{PSL}}(s) = J_{\mathrm{P}\theta-\mathrm{HP}}(s)\frac{k_p}{s}. \tag{40}$$

Fig. 6 shows that the PSL has a lower bandwidth and less phase margin with higher load angles θ_0. The reason is, as previously explained, that the RHP zero of the plant moves closer to the origin with higher load angles θ_0, as shown in Fig. 4.

From the open-loop transfer function $H_{\mathrm{PSL}}(s)$ in (40), the closed-loop transfer function of PSL can be derived

$$CL_{PSL}(s) = \frac{H_{PSL}(s)}{1 + H_{PSL}(s)} = \frac{k_p J_{\mathrm{P}\theta-\mathrm{HP}}(s)}{s + k_p J_{\mathrm{P}\theta-\mathrm{HP}}(s)}. \tag{41}$$

Comparing (41) to (40), it is easily observed that the RHP zero in the open-loop transfer function $H_{\mathrm{PSL}}(s)$ carries over to the closed-loop transfer function $CL_{\mathrm{PSL}}(s)$, i.e., the feedback control does not affect the location of the RHP zero.

B. Transfer Function of Reactive Power versus Voltage Magnitude

The derivation procedure of the transfer function between reactive power and voltage magnitude is similar to the procedure used for the derivation of the transfer function between active power and load angle. In this case, it is assumed $\theta = \theta_0$. However, V is allowed to vary. Thus

$$V = V_0 + \Delta V. \tag{42}$$

The d and q components of the current vector are kept as

$$i_d = i_{d0} + \Delta i_d, \qquad i_q = i_{q0} + \Delta i_q. \tag{43}$$

Equation (15) can now be linearized around the operating point V_0. Accordingly

$$L\frac{d\Delta i_d}{dt} = \Delta V\cos\theta_0 - R\Delta i_d + \omega_1 L\Delta i_q$$
$$L\frac{d\Delta i_q}{dt} = \Delta V\sin\theta_0 - R\Delta i_q - \omega_1 L\Delta i_d. \qquad (44)$$

Moreover, by applying the Laplace transform on (44), the following transfer functions between Δi_d, Δi_q, and Δv are obtained:

$$\Delta i_d = \frac{\omega_1 L\sin\theta_0 + (sL+R)\cos\theta_0}{(sL+R)^2+(\omega_1 L)^2}\Delta V$$
$$\Delta i_q = \frac{-\omega_1 L\cos\theta_0 + (sL+R)\sin\theta_0}{(sL+R)^2+(\omega_1 L)^2}\Delta V. \qquad (45)$$

Assuming p.u. quantities, the instantaneous reactive power is given by

$$Q = \mathrm{Im}\{\mathbf{v}\mathbf{i}^*\}. \qquad (46)$$

Linearizing (46) yields the following expression for the reactive-power deviation:

$$\Delta Q = \mathrm{Im}\{\mathbf{i}_0^*\Delta\mathbf{v} + \mathbf{v}_0\Delta\mathbf{i}^*\} \qquad (47)$$

or in component form

$$\Delta Q = \begin{bmatrix} I_{d0} \\ -I_{q0}\end{bmatrix}^{\mathrm{T}}\begin{bmatrix}\Delta v_q \\ \Delta v_d\end{bmatrix}] + \begin{bmatrix}V_{d0}\\ V_{q0}\end{bmatrix}^{\mathrm{T}}\begin{bmatrix}-\Delta i_q \\ \Delta i_d\end{bmatrix}. \qquad (48)$$

The operating points I_{d0}, I_{q0} and V_{d0}, V_{q0} are determined in the same way as in the case of the transfer function between active power and load angle. The same holds for Δv_d and Δv_q. By substituting (24), (25), (26), and (45) into (48), the reactive-power versus voltage-magnitude transfer function is obtained as

$$\Delta Q = \underbrace{\frac{a_0 s^2 + a_1 s + a_2}{(sL+R)^2+(\omega_1 L)^2}}_{J_{\mathrm{QV}}(s)}\Delta V \qquad (49)$$

where

$$a_0 = \frac{L}{\omega_1}(V_0 - E_0\cos\theta_0)$$
$$a_1 = \frac{R}{\omega_1}(V_0 - E_0\cos\theta_0)$$
$$a_2 = \omega_1 L(2V_0 - E_0\cos\theta_0) + RE_0\sin\theta_0. \qquad (50)$$

Obviously, $J_{\mathrm{QV}}(s)$ has the same poles as $J_{\mathrm{P}\theta}(s)$, i.e., similar to controlling active power by load angle, (49) shows that, by using voltage magnitude to control reactive power, the open-loop system has a pair of resonant (complex) poles

$$s = -\frac{R}{L} \pm j\omega_1. \qquad (51)$$

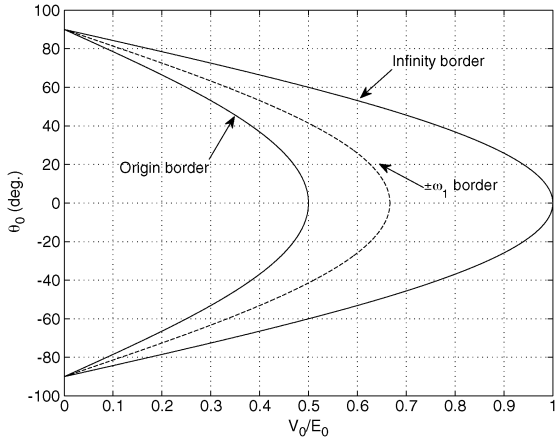

Fig. 7. Locations of zeros of $J_{\mathrm{QV}}(s)$.

By neglecting the resistance R, the two zeros of $J_{\mathrm{QV}}(s)$ are located at:

$$s = \pm\sqrt{-\frac{a_2}{a_0}} = \pm\omega_1\sqrt{\frac{2V_0 - E_0\cos\theta_0}{E_0\cos\theta_0 - V_0}}. \qquad (52)$$

Fig. 7 shows the locations of zeros of $J_{\mathrm{QV}}(s)$. Similar to $J_{\mathrm{P}\theta}(s)$, the origin border of $J_{\mathrm{QV}}(s)$ also indicates the stability border. By crossing the origin, the VSC can no longer control reactive power by means of the voltage magnitude, since an increased voltage magnitude ΔV will cause a decreased reactive power ΔQ. In contrast to the dynamics of $J_{\mathrm{P}\theta}(s)$, where the load angle θ_0 is the dominant factor for stability, the VSC voltage V_0 instead is the dominant factor for stability in the case of $J_{\mathrm{QV}}(s)$. It is also interesting to notice that the quasi-static (8) is a special case of (49) if $R = 0$ and $s = 0$ are substituted into (49).

By having the reactive-power versus voltage-magnitude transfer function $J_{\mathrm{QV}}(s)$ and the reactive-power control law, it is also possible to evaluate the stability margin of the reactive power control in a similar way as for the power-synchronization loop.

The analysis in this section is based on a simplified VSC-ac-system model. The aim is to derive the analytical transfer functions to understand the fundamental dynamic process for VSC-HVDC connected to weak ac systems. In real applications, the ac system topology is much more complex, and contains other dynamic devices, such as generators, compensation equipment, and loads, which could interact dynamically with VSC-HVDC, too. As observed in this section, the derivation of the transfer functions for this simplified system is already cumbersome. Thus, it is not realistic to derive the explicit transfer functions for more complex systems. However, numerical analysis based on state-space representation of the system for evaluation of VSC-control stability margins is easily performed for much larger systems. Besides, when both the power-synchronization loop and the reactive-power control are active, the system is in principle of multi-input multi-output (MIMO) nature. Therefore, MIMO analyzing and control techniques should be applied to achieve optimal control results. These issues certainly require in-depth investigations in the future.

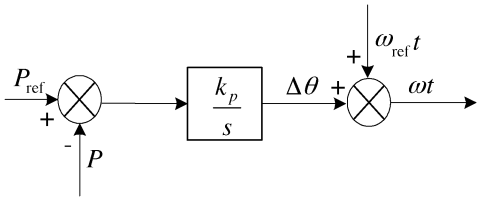

Fig. 8. Power-synchronization loop.

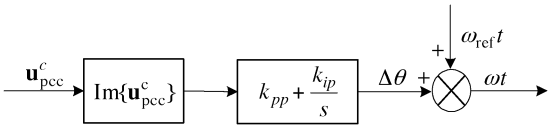

Fig. 9. Backup phase-locked loop.

IV. Controller Design

In this section, the overall control design of VSC-HVDC based on power synchronization is described.

A. Power-Synchronization Loop (PSL)

This is the fundamental control loop for a grid-connected VSC based on power-synchronization control. It maintains synchronism between the VSC and the ac system, and at the same time, it is also the active-power control loop. Fig. 8 shows the block diagram of the power-synchronization loop. The power control error is converted to a frequency deviation, which is then integrated to an angle increment. The output signal ωt supplies the angle to transform the voltage reference $\mathbf{v}^c_{\text{ref}}$ from the converter dq frame to the stationary frame.

B. Backup Phase-Locked Loop (PLL)

In some situations, the PSL cannot be applied, and the backup PLL is used instead. Those situations are as follows.

- The VSC is blocked. The backup PLL provides the synchronization signal to the VSC before de-blocking. After the converter is de-blocked, the PLL is replaced by the PSL. This procedure is similar to the auto-synchronization process used for synchronous generators before they are connected to the grid.
- During severe ac-system faults, the control system switches to the backup PLL. The reason is that the control system has to limit the current flowing into the converter valve. Thus, the PSL cannot be applied. The current limitation function will be described in Section IV-F.

Fig. 9 shows the block diagram of the backup PLL, where a proportional-plus-integral (PI) type regulator is applied upon the error signal coming from the imaginary part of the voltage $\mathbf{u}^c_{\text{pcc}}$ at the PCC in the converter dq frame.

C. Direct-Voltage Controller (DVC)

In VSC-HVDC applications, one of the converter stations has to keep the direct voltage constant, while the other converter station controls the active power. The active power is thus automatically balanced between the two stations. If the direct-voltage controller were to operate directly on the error $v^{\text{ref}}_{\text{dc}}-v_{\text{dc}}$, the closed-loop dynamics would be dependent on the operating point v°_{dc}. This inconvenience is avoided by selecting the direct-voltage controller (DVC) as a PI controller operating instead on the error $[(v^{\text{ref}}_{\text{dc}})^2-v^2_{\text{dc}}]/2$ [11], [16]. The control law of the DVC is thus described by

$$P_{\text{ref}}=\left(k_{pd}+\frac{k_{id}}{s}\right)\frac{\left(v^{\text{ref}}_{\text{dc}}\right)^2-v^2_{\text{dc}}}{2}. \tag{53}$$

The output of the DVC provides the power reference P_{ref} to the PSL. Fig. 10 shows the control block diagram.

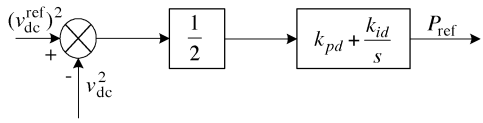

Fig. 10. Direct-voltage controller.

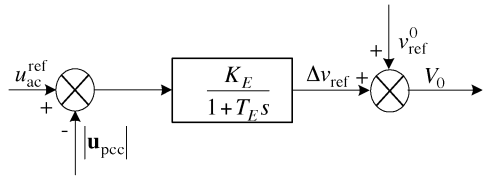

Fig. 11. Alternating-voltage controller.

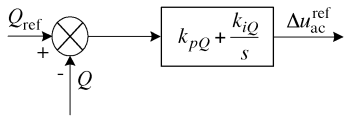

Fig. 12. Reactive-power controller.

D. Alternating-Voltage Controller (AVC)

In VSC-HVDC applications, especially in connection with weak ac systems, the VSC control system should preferably maintain the alternating-voltage level at the PCC. Fig. 11 shows the control block diagram of the AVC. The output of the AVC supplies the voltage reference to voltage control law of the VSC. The AVC is designed as a proportional controller to have a "droop" characteristic. However, if other voltage controlling devices, such as STATCOMs, or synchronous generators are present in the close proximity, it has been found that an additional droop function is necessary.

E. Reactive-Power Controller (RPC)

When operating against a weak ac system, the VSC-HVDC should preferably be operated in the alternating-voltage control mode to give the ac system best possible voltage support. In case reactive-power control is necessary, the output of this controller should be added to the alternating-voltage reference, and the added amount should be limited. Fig. 12 shows the block diagram of the RPC, and the output of the RPC is added to the voltage reference of the AVC.

F. Current-Limitation Controller (CLC)

A shortcoming of the power-synchronization control is that the alternating current at the fundamental frequency is not con-

trolled, since the current control conflicts with the power-synchronization mechanism, as explained in Section II-B. However, for VSC applications, it is important to limit the current flowing into the converter valve to prevent the valve from over-current blocking. In this section, therefore, a current limitation scheme is proposed. The principle is to seamlessly switch the control system to vector-current control to avoid triggering of the over-current protection circuit. At the same time, the backup PLL is applied to keep the VSC in synchronism with the ac system.

In case that the current through the valve is above its limit $I_{\max}$, the desired voltage control law of the VSC is given by

$$\mathbf{v}_{\text{ref}}^{c} = \alpha_c L_c \left(\mathbf{i}_{\text{ref}}^{c} - \mathbf{i}^{c}\right) + j\omega_1 L_c \mathbf{i}^{c} + \mathbf{u}_{f}^{c} \tag{54}$$

where α_c is the desired closed-loop bandwidth of the current control, $\mathbf{i}_{\text{ref}}^{c}$ is the converter current reference, and $\mathbf{u}_{f}^{c}$ is a low-pass filtered feedforward term of the PCC voltage $\mathbf{u}_{\text{pcc}}^{c}$. Equation (54) is the voltage control law given by the vector controller for the current. However, instead of giving constant current order to (54), the current reference $\mathbf{i}_{\text{ref}}^{c}$ in (54) is given as

$$\mathbf{i}_{\text{ref}}^{c} = \frac{1}{\alpha_c L_c}\left[V_0 - \mathbf{u}_{f}^{c} - j\omega_1 L_c \mathbf{i}^{c} - H_{\text{HP}}(s)\mathbf{i}^{c}\right] + \mathbf{i}^{c}. \tag{55}$$

The current reference (55) is designed in such a way that the voltage control law (54) becomes (36) for power-synchronization control in normal operation. This can easily be shown by substituting (55) in (54). However, the current reference $\mathbf{i}_{\text{ref}}^{c}$ in (55) gives an indication of the real current flowing into the converter valve. During ac system faults, current limitation is automatically achieved by limiting the modulus of $\mathbf{i}_{\text{ref}}^{c}$ to the maximum current $I_{\max}$. A brief analysis of this is given below.

The dynamics of the converter current in the converter dq frame can be described by

$$L_c \frac{d\mathbf{i}^{c}}{dt} = \mathbf{v}^{c} - \mathbf{u}_{\text{pcc}}^{c} - R_c \mathbf{i}^{c} - j\omega_1 L_c \mathbf{i}^{c}. \tag{56}$$

Assuming $\mathbf{v}^{c} = \mathbf{v}_{\text{ref}}^{c}$, (56) can be substituted with (54). Accordingly

$$L_c \frac{d\mathbf{i}^{c}}{dt} = \alpha_c L_c \left(\mathbf{i}_{\text{ref}}^{c} - \mathbf{i}^{c}\right) + \mathbf{u}_{f}^{c} - \mathbf{u}_{\text{pcc}}^{c} - R\mathbf{i}_{c}^{c}. \tag{57}$$

By setting the time derivative to zero and assuming that $\mathbf{u}_{\text{pcc}}^{c} = \mathbf{u}_{f}^{c}$, it is found that

$$\mathbf{i}^{c} = \frac{\alpha_c L_c}{R_c + \alpha_c L_c}\mathbf{i}_{\text{ref}}^{c} \Rightarrow \left|\mathbf{i}^{c}\right| \le \left|\mathbf{i}_{\text{ref}}^{c}\right|. \tag{58}$$

As R_c is usually much smaller than $\alpha_c L_c$, the modulus of the valve current will be almost equal to the modulus of the current reference. In other words, by limiting the modulus of the current reference, the current flowing into the converter valve is limited. Fig. 13 shows the control block diagram. In Fig. 13, the "Current Reference Control" block corresponds to the control law described by (55), while the "Voltage Control" block corresponds to the control law described by (54). If the modulus

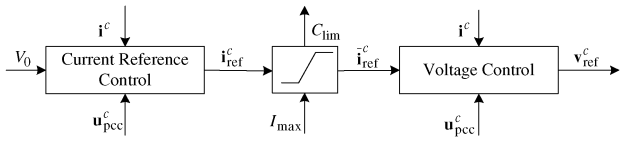

Fig. 13. Current limitation controller.

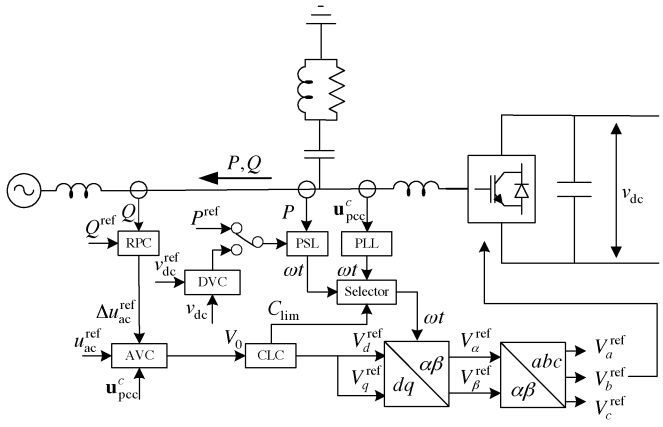

Fig. 14. VSC-HVDC control overview.

of the current reference $\mathbf{i}_{\text{ref}}^{c}$ is above the current limit $I_{\max}$, it will be reduced to a vector $\bar{\mathbf{i}}_{\text{ref}}^{c}$, whose modulus is equal to $I_{\max}$ (priority might be given to i_{dref}^{c} or i_{qref}^{c} depending on the control design). Once $\mathbf{i}_{\text{ref}}^{c}$ is limited, the CLC will also send a signal C_{lim} to the main control system for the PSL/PLL selection.

Fig. 14 shows an overview of the VSC controller based on power-synchronization control. The overview illustrates the relationships between the various controllers mentioned in this section.

V. Simulation Results

To verify the control design and the analytical model, a VSC-HVDC link is built in the time simulation software PSCAD/EMTDC. The simulation setup contains a VSC-HVDC link sending power to a 400-kV ac system with a short-circuit ratio (SCR) of 1.0. The other end of the VSC-HVDC link is assumed to be a strong ac system. The parameters of the VSC are listed in the Appendix.

A. Effect of the High-Pass Current Control Part

As shown in Section III, for both the dynamics in $J_{\text{P}\theta}(s)$ and $J_{\text{QV}}(s)$, there is a pair of resonant poles at the grid frequency. A high-pass current control part $H_{\text{HP}}(s)$ was proposed to provide active damping to the system. Fig. 15 demonstrates the effect of $H_{\text{HP}}(s)$ in a time simulation. After the high-pass current control part $H_{\text{HP}}(s)$ is disabled at approximately 0.05 s, the resonance is excited by an active power (P) step (0.1 p.u.) at 0.1 s. The high-pass current control part is enabled again at 0.35 s, and damps out the resonance effectively. The time simulation results confirm (38) and the corresponding Bode diagram in Fig. 6. The observed resonance frequency is slightly lower than the grid frequency 50 Hz. This deviation is not unexpected, since the observed resonance frequency is the damped frequency, which is always lower than the undamped natural frequency 50 Hz.

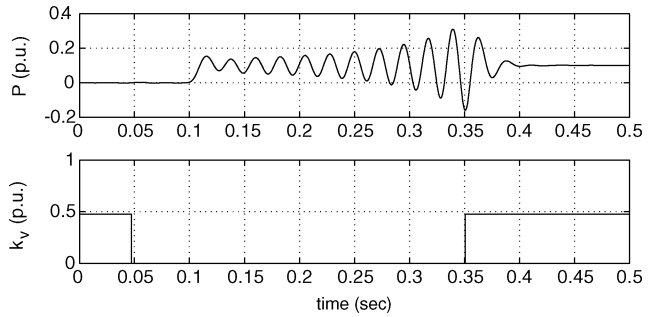

Fig. 15. Grid-frequency resonance and the effect of high-pass current control part $H_{\mathrm{HP}}(s)$, $k_v = 0.477$ p.u., $\alpha_v = 40$ p.u./s.

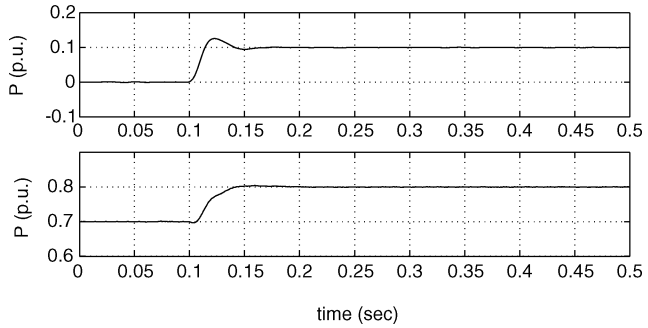

Fig. 16. Active power (P) step response at low load angle (upper plot) and high load angle (lower plot) with power-synchronization control.

B. Step-Response Tests With Low Load Angle and High Load Angle

Two active-power step-response tests (0.1 p.u.) are performed at a low load angle and a high load angle, respectively. According to the open-loop transfer function of the power-synchronization loop (40), and its Bode diagram in Fig. 6, the system exhibits a reduced phase margin at high load angles, but at the same time, $J_{\mathrm{P}\theta}(s)$ also has a lower open-loop gain. Thus, the step response at high load angle is slower but not particularly unstable, as shown by the plot in Fig. 16. A slight non-minimum-phase behavior (the active power P slightly goes down before it responds to the positive step), typically accompanying RHP zeros, is also observed for the step response at high load angle. This is due to the fact that the RHP zero moves closer to the origin with higher load angle, as previously explained.

C. Fault Ride-Through Capability

The fault ride-through capability of the VSC-HVDC system is tested by applying a three-phase ac fault close to the VSC-HVDC. The VSC initially operates with a power of 0.8 p.u., which corresponds to a load angle of approximately 65°. It is to be stressed that, even though VSC-HVDC based on power-synchronization control theoretically is able to maintain operation at a load angle close to 90°, higher load angles than 70° are not recommended. The reason is that the stability margin is dramatically reduced at higher load angles, while not much transmitted power is gained (less than 0.06 p.u. between 70° and 90°).

In Fig. 17, the ac-system fault is applied at 0.1 s, and the modulus of the current reference ($|\mathbf{i}^c_{\mathrm{ref}}| = \sqrt{(i^c_{\mathrm{dref}})^2 + (i^c_{\mathrm{qref}})^2}$) reaches the current limit $I_{\max}$. The control system seamlessly

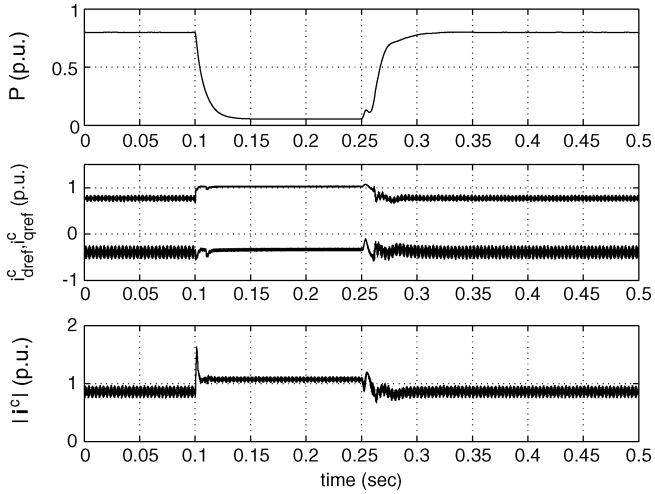

Fig. 17. Fault ride-through capability of VSC-HVDC during a three-phase ac fault with power-synchronization control.

switches to the voltage control law (54), where the limited i^c_{dref} and i^c_{qref} become the inputs to the current controller. Only a short current spike lasting for approximately 10 ms is observed on the valve current $|\mathbf{i}^c|$ at the fault occurrence stage, which usually does no harm to the converter valve. At the same time, the PSL is replaced by the backup PLL. After the fault is cleared at 0.25 s, the current reference i^c_{dref} and i^c_{qref} go back to the pre-fault level, and the voltage-control law switches back to (36). At the same time, the control system switches back to the PSL from the backup PLL. It is to be noted that, during ac system faults, the switching of the VSC voltage-control law between (54) and (36) is done seamlessly. However, the switching from the PSL to the backup PLL, and back to the PSL after fault clearance, is done by the control system based on fault detection logic. Otherwise, the PSL would accelerate the "rotor speed" of the VSC-HVDC during the ac system fault, and run into a transient stability problem as a normal synchronous machine after the ac system fault is cleared. Physically, VSC-HVDC using power-synchronization control could be understood as a synchronous machine which is able to limit its short-circuit current contribution and keep its "rotor" running at normal speed during ac system faults.

D. Comparison to Vector-Current Control

In order to demonstrate the effectiveness of power-synchronization control, a comparison to vector-current control with a PLL has been performed based on simulations. In this case, (54) was used with I^c_{dref} provided by a PI-type power controller for the d-component and by a PI-type voltage controller for the q-component. The case with 0.8 p.u. of power could not be handled with vector-current control. In fact, it is known from the literature, for instance [9], that it is not possible to operate a VSC with vector-current control and PLL synchronization at a higher power than approximately 0.4 p.u. if the SCR of the ac system is 1.0. However, after a considerable tuning effort, it was possible to achieve a step from 0.5 p.u. to 0.6 p.u., which is shown in Fig. 18 as a comparison to Fig. 16.

The case with a three-phase ac fault with 0.6 p.u. pre-fault power level was simulated using vector-current control. The

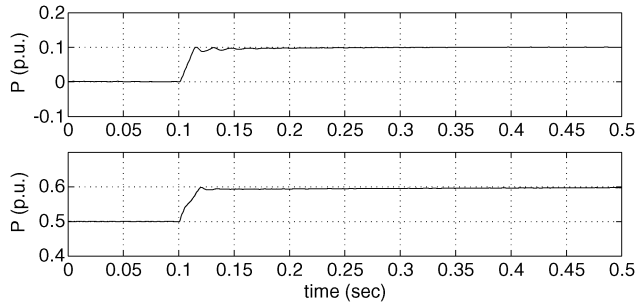

Fig. 18. Active power (P) step response at low load angle (upper plot) and high load angle (lower plot) with vector-current control.

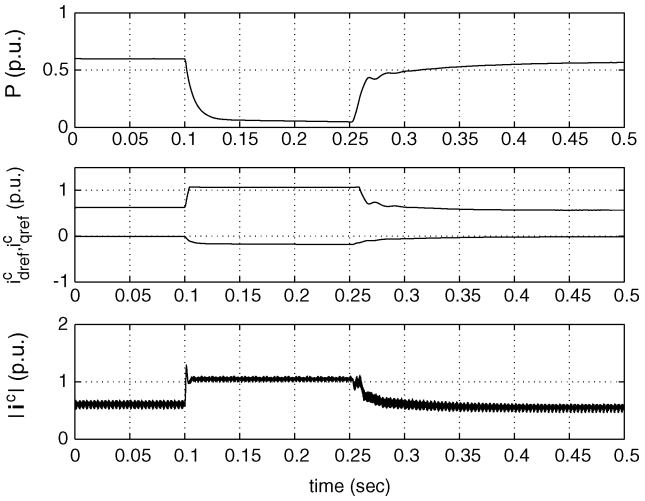

Fig. 19. Fault ride-through capability of VSC-HVDC during a three-phase ac fault with vector-current control.

fault recovery could only be achieved after a considerable retuning of the voltage controller and the power controller in order to avoid a "voltage collapse." Note that these new parameter sets were selected to fit only this specific case. The simulated results are shown in Fig. 19 as a comparison to Fig. 17.

VI. Conclusions

In this paper, the concept of power synchronization is proposed for control of grid-connected VSCs. The proposed control is general for grid-connected VSCs, but may be of most importance for VSC-HVDC connected to weak ac systems. By using the power-synchronization control method, VSC-HVDC operates almost in the same way as a synchronous machine. Therefore, in principle, it has no requirement on the short-circuit capacity of the ac system to be connected. On the other hand, VSC-HVDC gives the weak ac system strong voltage support, just like a normal synchronous machine does. However, a weak ac system connection still represents a more challenging operating condition for VSC-HVDC than a strong ac system connection due to the relatively higher load angles. Thus, it is recommended that VSC-HVDC shall run with a control system having a lower bandwidth when connected to a very weak ac system in order to maintain a safe stability margin.

TABLE I
VSC-HVDC System Parameters

Rated apparent power $S_{\rm sys}$	350.0 MVA	1.0 p.u.
Rated (base) voltage $U_{\rm b}$	195.0 kV	1.0 p.u.
Maximum valve current $I_{\rm max}$	1.12 kA	1.08 p.u.
Phase reactor inductance	0.052 H	0.15 p.u.
Phase reactor resistance	0.06 Ω	0.0055 p.u.
Converter transformer rating	380.0 MVA	
Converter transformer ratio	195 kV/400 kV	
Transformer leakage reactance	12%	0.11 p.u.
Direct voltage $v_{\rm dc}$	±150.0 kV	1.0 p.u.
DC capacitor	114 μF	
System frequency f	50 Hz	
Switching frequency $f_{\rm sw}$	1650 Hz	

Appendix

A. Parameters of the VSC-HVDC System

Table I lists the VSC-HVDC system parameters.

Acknowledgment

The authors would like to thank G. Asplund and Y. J. Häfner for helpful discussions in forming the idea of power synchronization.

References

[1] J. Holtz, "Pulsewidth modulation for electronic power conversion," *Proc. IEEE*, vol. 82, no. 8, pp. 1194–1214, Aug. 1994.
[2] G. Asplund, K. Eriksson, and H. Jiang, "DC transmission based on voltage source converters," in *Proc. Cigre Conf. 14-302*, Paris, France, 1998.
[3] J. Svensson, "Grid-connected voltage source converter," Ph.D. dissertation, Chalmers Univ. Technol., Gothenburg, Sweden, 1998.
[4] B. T. Ooi and X. Wang, "Voltage angle lock loop control of the boosted type PWM converter for HVDC application," *IEEE Trans. Power Electron.*, vol. 5, no. 2, pp. 229–235, Apr. 1990.
[5] G. Joos, L. Moran, and P. Ziogas, "Performance analysis of a PWM inverter VAR compensator," *IEEE Trans. Power Electron.*, vol. 6, no. 3, pp. 380–391, Jul. 1991.
[6] J. Svensson, "Voltage angle control of a voltage source inverter, application to a grid-connected wind turbine," in *Proc. 6th Eur. Conf. Power Electronics and Applications*, Sevilla, Spain, 1995.
[7] P. Fischer, "Modelling and control of a line-commutated HVDC transmission system interacting with a VSC STATCOM," Ph.D. dissertation, Royal Inst. Technol., Stockholm, Sweden, 2007.
[8] M. P. Kazmierkowski and L. Malesani, "Current control techniques for three-phase voltage-source PWM converters: A survey," *IEEE Trans. Ind. Electron.*, vol. 45, no. 5, pp. 691–703, Oct. 1998.
[9] M. Durrant, H. Werner, and K. Abbott, "Model of a VSC HVDC terminal attached to a weak ac system," in *Proc. IEEE Conf. Control Applications*, Istanbul, Turkey, 2003.
[10] H. Konishi, C. Takahashi, H. Kishibe, and H. Sato, "A consideration of stable operating power limits in VSC-HVDC systems," in *Proc. 7th Int. Conf. AC-DC Power Transmission*, London, U.K., 2001.
[11] L. Harnefors, M. Bongiornos, and S. Lundberg, "Input-admittance calculation and shaping for controlled voltage-source converters," *IEEE Trans. Ind. Electron.*, vol. 54, no. 6, pp. 3323–3334, Dec. 2007.
[12] J. Svensson, "Synchronisation methods for grid-connceted voltage source converters," *Proc. Inst. Elect. Eng., Gen., Transm., Distrib.*, vol. 148, no. 3, pp. 229–235, May 2001.
[13] D. Jovcic, L. A. Lamont, and L. Xu, "VSC transmission model for analytical studies," in *Proc. IEEE Power Eng. Soc. General Meeting*, Toronto, ON, Canada, 2003.

[14] D. Lee, "Voltage and power stability of HVDC systems," Ph.D. dissertation, Royal Inst. Technol., Stockholm, Sweden, 1997.
[15] S. Skogestad and I. Postlethwaite, *Multivariable Feedback Control*, 2nd ed. New York: Wiley, 2005, pp. 183–187.
[16] R. Ottersten, "On control of back-to-back converters and sensorless induction machine drives," Ph.D. dissertation, Chalmers Univ. Technol., Gothenburg, Sweden, 2003.

Lidong Zhang (M'07) received the B.Sc. degree from the North China Electric Power University, Baoding, China, in 1991 and the Tech.Lic degree from Chalmers University of Technology, Gothenburg, Sweden, in 1999. Since 2007, he has been pursuing the Ph.D. degree part-time in the Royal Institute of Technology, Stockholm, Sweden.

From 1991 to 1996, he worked as an engineer with the Leda Electric Co., Beijing, China. Since 1999, he has been with ABB Power Systems, Ludvika, Sweden. His research interests are HVDC, power system stability and control, and power quality.

Lennart Harnefors (S'93–M'97–SM'07) was born in 1968 in Eskilstuna, Sweden. He received the M.Sc., Licentiate, and Ph.D. degrees in electrical engineering from the Royal Institute of Technology, Stockholm, Sweden, and the Docent (D.Sc.) degree in industrial automation from Lund University, Lund, Sweden, in 1993, 1995, 1997, and 2000, respectively.

From 1994 to 2005, he was with Mälardalen University, Västerås, Sweden, where he, in 2001, was appointed as a Professor of electrical engineering. He is currently with ABB Power Systems, Ludvika, Sweden. Since 2001, he is also a part-time Visiting Professor of electrical drives at Chalmers University of Technology, Gothenborg, Sweden. His research interests include applied signal processing and control, in particular, control of power electronic systems and ac drives.

Prof. Harnefors was the recipient of the 2000 ABB Gunnar Engström Energy Award and the 2002 IEEE TRANSACTIONS ON INDUSTRIAL ELECTRONICS Best Paper Award. He is an Associate Editor of the IEEE TRANSACTIONS ON INDUSTRIAL ELECTRONICS.

Hans-Peter Nee (S'91–M'96–SM'04) was born in 1963 in Västerås, Sweden. He received the M.Sc., Licentiate, and Ph.D degrees in electrical engineering from the Royal Institute of Technology, Stockholm, Sweden, in 1987, 1992, and 1996, respectively.

He was appointed Professor of power electronics in the Department of Electrical Engineering at the Royal Institute of Technology in 1999. His interests are power electronic converters, semiconductor components and control aspects of utility applications, like FACTS and HVDC, and variable-speed drives.

Prof. Nee was awarded the Energy Prize by the Swedish State Power Board in 1991, the ICEM'94 (Paris) Verbal Prize in 1994, the Torsten Lindström Electric Power Scholarship in 1996, and the Elforsk Scholarship in 1997. He has served in the board of the IEEE Sweden Section for many years and was the chairman of the board during 2002 and 2003. He is also a member of EPE and serves in the Executive Council and in the International Steering Committee. Additionally, he is active in IEC and the corresponding Swedish organization SEK in the committees TC 25 and TK 25, respectively.